SANDIA REPORT SAND83—2576 • Unlimited Release • UC—45
Printed April, 1984

A Thin Flame Model for Reactive Flow in Porous Materials

M. R. Baer, J. E. Shepherd

Prepared by
Sandia National Laboratories
Albuquerque, New Mexico 87185 and Livermore, California 94550
for the United States Department of Energy
under Contract DE-AC04-76DP00789

SF2900Q(8-81)

Issued by Sandia National Laboratories, operated for the United States Department of Energy by Sandia Corporation.

Printed in the United States of America
Available from
National Technical Information Service
U.S. Department of Commerce
5285 Port Royal Road
Springfield, VA 22161

NTIS price codes
Printed copy: A04
Microfiche copy: A01

Distribution
Category UC–45

SAND83-2576
Unlimited Release
Printed April, 1984

A Thin Flame Model for Reactive Flow in Porous Materials

M. R. Baer
Fluid Mechanics and Heat Transfer Division, 1513

J. E. Shepherd
Fluid Mechanics and Heat Transfer Division, 1512

Sandia National Laboratories
Albuquerque, New Mexico 87185

ABSTRACT

In this report we present a model for the flow processes associated with a gas-generating combustion wave propagating through a porous reactor. A one-dimensional model is constructed using a thin flame approximation. The flow is determined by the permeability of the unreacted material and the exothermicity of the combustion. Numerical calculations are presented to demonstrate various aspects of the model. In addition, analytical solutions to the flow fields are determined for the limiting cases of reactants with very high or low permeability.

Acknowledgements

We gratefully acknowledge the many fruitful discussions with W. Hermina, G. Evans, M. Johns, S. Griffiths and A. Reed. We also extend our appreciation to J. Nunziato and D. Hayes for their encouragement and support during the course of this investigation.

Contents

Figures

1 Introduction

In this study, we present a simple model for one-dimensional propagation of a combustion wave in reactive, gas-permeable materials. In particular, we examine the combustion of a heterogeneous mixture of granulated, solid reactant which forms a solid residue and hot combustion-product gases. Our model is applicable to slow combustion and is an analog of approximate flame-sheet models developed for gaseous combustion [1, 2]. Utilizing the thin-flame approximation greatly simplifies the calculation since the detailed structure of the flame is eliminated. This removes a major source of difficulty in the computations by separating the vastly different length and time scales associated with the flame structure and those associated with flow processes outside the flame. Without the thin-flame assumption, fast reaction kinetics produce a high degree of stiffness in the system of differential equations used to model the problem and a high-resolution spatial grid must be used in the vicinity of the flame. Development of efficient numerical methods for such problems is an area of intense current research and an interim technique which eliminates these difficulties would be quite useful for parametric engineering studies.

As in the gaseous combustion models, the present study treats the combustion wave as a density and temperature discontinuity. The states upstream and downstream of the combustion wave are related by jump conditions to assure the conservation of mass, momentum and energy. The combustion physics is introduced in the model by prescribing a burn velocity of the combustion wave discontinuity. The burn velocity, or "flame law", can be treated as a function of pressure, temperature or concentration at the flame front , as determined by experiments. Alternatively, if sufficient knowledge of reaction mechanisms, rates and transport processes is known, the burn velocity can be calculated by a separate, two-point boundary value computation – a procedure which has been used previously in single- and two-phase combustion [3 - 5]. In addition to the burn velocity, the flow resistance of the unburned porous material and the thermodynamic properties of the reaction products must be estimated or measured.

In the sections to follow, we will outline the details of the proposed model. Our model divides the flow field into three regions: a postcombustion zone composed of high-pressure gaseous combustion products and solid residue; a thin flame/preheat zone in which all combustion and thermal nonequilibrium

effects occur; and a zone of unburned porous reactant into which the gaseous combustion products permeate.

Simplifying assumptions are introduced and described for each region. With these assumptions, a model is constructed which consists of a single partial differential equation and boundary conditions. To illustrate the features of this model, numerical solutions are found for the flow induced by a combustion wave which propagates at a constant velocity from the closed end of a finite-length column of reactant toward an open end which vents gaseous combustion product to ambient pressure. We will show that the character of the flow field described by this model is completely determined by two nondimensional parameters. For two extremes, corresponding to very large and very small permeability of the unreacted porous media, analytical solutions to the governing flow equations are derived. In addition, an approximate solution method to internal pressure distributions and exit flow rate are then compared to numerical solutions.

In the final section and appendices of this report, we suggest various extensions to our basic model. These extensions would allow more general treatment of the combustion aspect of this problem and enhance its overall utility as an engineering tool.

2 Overview of Model and Assumptions

To illustrate our model, consider a one-dimensional, porous flow reactor in which a combustion wave is initiated at the closed end of a vessel (see Figure 1). Gas generation is a result of the overall reaction occurring within the combustion zone:

$$Solid_1 + Solid_2 \rightarrow Solid\,(alloy) + Gas + Heat. \qquad (1)$$

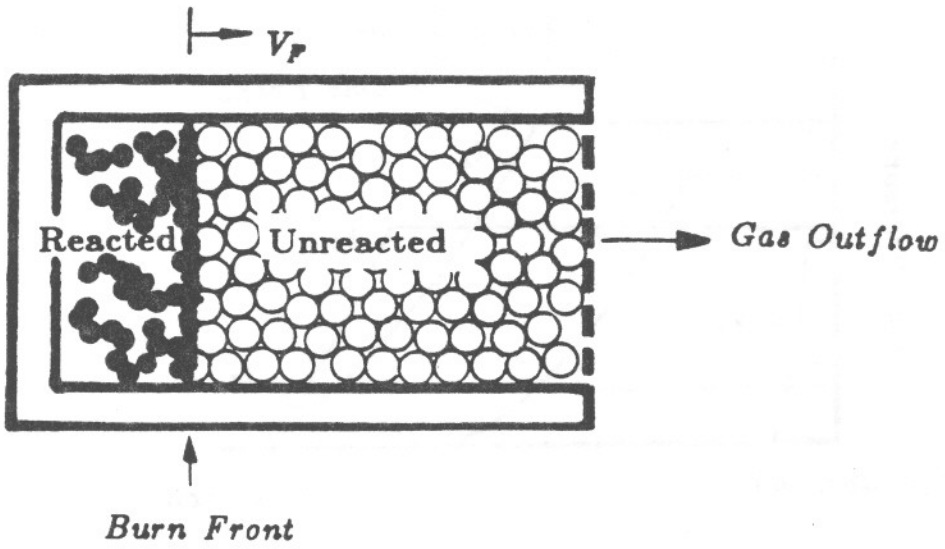

Figure 1. Pictorial of a one-dimensional porous reactor.

The exact composition of the reactants and products is unimportant to the present study, and our results are intended to apply to any system of this sort as long as the reaction zone can be considered to be thin compared to the length of the reactant column and the combustion is slow (*i.e.* , the burn velocity is much less than the sound speed in the reactant material). If a melt phase is present during combustion, our model will be applicable only if the melt is confined to the combustion zone and solidifies rapidly outside of it.

Due to the confining effect of the reactor vessel and frictional forces restraining the unreacted material, a pressure gradient is quickly established following ignition and gas flows through the unreacted medium. If the gas generation rate at the combustion front exceeds the rate of permeation into the unreacted porous material, a continual pressure buildup occurs in the reacted region. At some time following ignition, the gas permeation front in the unreacted material will arrive at the open end of the vessel and venting of the gas will occur. This venting process counteracts the pressure buildup in the reacted region and the pressure at the flame front will begin to decay. Thus, we expect that the evolution of the pressure distribution in the vessel is closely related to the flow processes occurring in the unreacted and reacted regions of the vessel. A schematic of this pressure development is shown in Figure 2.

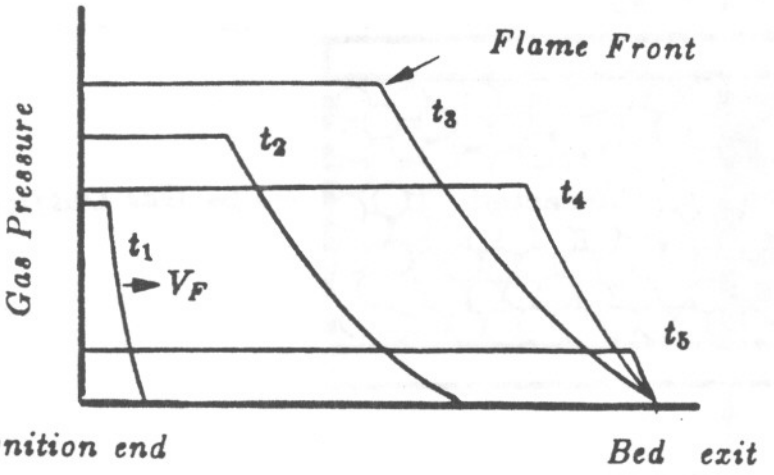

Figure 2. Anticipated behavior of pressure developed during combustion, $t_1 < t_2 < t_3 < t_4 < t_5$.

In the model to be described, we shall consider the porous material to be immobile; this limits the application of this model to porous materials that are packed tightly to withstand the forces associated with the highest possible pressure (adiabatic combustion overpressure) developed at the flame front. Furthermore, we will not consider mechanical compaction effects that are known to occur during flame spread in explosives [6]. This effect will cause pore collapse which can impede the permeation of the gas.

As we envision this combustion process, it is evident that three distinct regions must be considered: the reacted region between the closed end of the vessel and the flame; the flame/preheat zone in which all combustion and composition/thermal gradients occur; and, the unreacted zone between the flame and the open end of the vessel. In the sections to follow, we will examine each region in detail.

Reacted Zone

Combustion products (both solid residue and gas) accumulate in the region where combustion has occurred. If the combustion generates gaseous products at a rate exceeding the permeating flow ahead of the flame, gas remaining in the open pores of the product solid is compressed and the pressure increases.

Furthermore, if the residual solid is highly permeable the pressure within this region can be treated as being spatially uniform. Solid-solid reactions often have this property, since the agglomeration of particles and the density decrease of the solid following reaction causes a large increase in pore size and the development of fissures in the solid product.

The combustion products left behind the flame are considered to be in thermal equilibrium and fixed at a uniform temperature as dictated by adiabatic combustion. This equilibrium constraint is valid if the thermal capacitance of the solid residue far exceeds that of the combustion product gas. Large gas-to-solid heat transfer rates, typical of porous flow, will cause the compressional heating of the gas to be quickly absorbed by the reacted solid.

Flame/Preheat Zone

The next region is the flame/preheat zone containing the combustion reaction and thermal gradients. Thermal gradients are caused by conduction of heat from the combustion and convective heat transfer from the hot product gas which is forced into the cold unreacted material. The heat transfer between the hot product gas and the solid unreacted material occurs until the gas temperature reaches that of the unignited reactant. Thus, product gas exiting the preheat zone has equilibrated to the temperature of the cold unreacted material.

A fundamental assumption of our model is that the flame/preheat zone is very thin compared to the total length of combustion wave propagation. This assumption will be valid when the reaction kinetics are fast and the heat transfer occurring in the preheat zone is rapid. The reaction kinetics are a strong function of the specific reactants under consideration and validity of the fast reaction assumption must be determined for the case of interest. Heat transfer ahead of the flame occurs by both conduction and interphase convective heat exchange between the gas and solid phases. From fundamental combustion theory [7], the length of the preheat zone, $\hat{\delta}_{preheat}$, determined by conduction alone, can be estimated as:

$$\hat{\delta}_{preheat} \sim \frac{\hat{\alpha}}{\hat{V}_F}, \tag{2}$$

where $\hat{\alpha}$ is the thermal diffusivity of the porous unreacted material and $\hat{V}_F$ is the burn velocity of the combustion wave. For many combustion situations this region is small. For example, if we consider a typical metallic diffusivity of $\hat{\alpha} = 0.2\ cm^2/s$ and a burn velocity of $\hat{V}_F = 2\ cm/s$, the preheat zone is of the

order of a millimeter in thickness . (As in the above notation , we refer to all dimensional quantities by denoting them with a ˆ accent.)

To examine the convective preheating effect of hot gas permeation ahead of the flame zone one must consider interphasial heat transfer. If the solid reactant particles are sufficiently small so that a large specific surface area is available for heat transfer, rapid heat exchange will occur. In estimating this convective heat exchange, we use a model similar to that postulated by Schumann [8]. The interested reader is referred to Appendix A for a more complete development of this model. A convective heat transfer coefficient was estimated using an empirical correlation [9]. Using representative gas properties and a small particle diameter in this packed-bed correlation, a large exchange coefficient for the convective heat transfer is calculated and the resulting convective thermal boundary layer is much smaller than the conduction layer thickness given by equation (2).

Unreacted Zone

The remaining portion of the reactor is the zone of unreacted material into which cold product gas permeates. As discussed above, all of the thermal energy is extracted from the hot product gases in a narrow layer in front of the flame. Consequently, only the interphase momentum exchange between the solid unreacted material and the permeating gas must be considered in this zone. We use the Darcy approximation which balances the pressure gradients with drag forces. The permeability coefficient in this model must be estimated from known empirical laws or experimentally measured. In this study we have estimated this parameter using the Blake-Kozney relationship [10] which requires the local Reynolds number (based on interstitial velocity and pore hydraulic diameter) to be small. As will be discussed in a later section, this parameter is of major importance, suggesting that experimental determination of the permeability is an important step in applying the model to real systems [11].

3 Theory

Using the assumptions introduced in the previous sections, we now develop the fundamental governing equations which will describe the combustion-driven gas flow. First, we examine the jump relationships across the flame/preheat discontinuity.

Consider a control volume (shown in Figure 3) which moves at the combustion wave velocity, $\hat{V}_F$. This control volume contains the reaction/preheat zone which we will consider to be of a vanishing small volume. We denote conditions of the reacted and unreacted states by the superscripts b and u and the solid- and gas-phase quantites by the subscripts s and g.

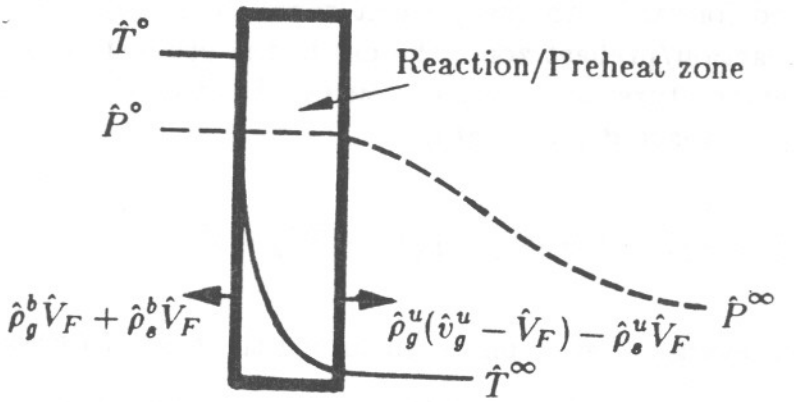

Figure 3. Control volume encompassing the reaction/preheat zone.

We introduce the partial density of each phase, $\hat{\rho}_i$, $(i = s, g)$, as the product of volume fraction, ϕ_i , times the material density, $\hat{\Gamma}_i$:

$$\hat{\rho}_i = \phi_i \hat{\Gamma}_i. \tag{3}$$

As indicated in Figure 3, the mass generation rate of gas is equal to the change in solid partial density times the burn velocity. A fraction of the gas is forced forward into the unreacted porous material and the remainder is left in the reacted region. Therefore, the balance of mass is simply stated as:

$$\hat{\rho}_g^u \hat{v}_g^u = \hat{V}_F(\hat{\rho}_s^u - \hat{\rho}_s^b) + \hat{V}_F(\hat{\rho}_g^u - \hat{\rho}_g^b), \tag{4}$$

where $\hat{v}_g$ is the average interstitial gas velocity relative to a laboratory reference frame. (Note that the gas flow into the reacted region is absent. This is due to the assumption of negligible flow resistance in the reacted region.)

Next, we consider the balance of momentum across the discontinuity. Ignoring inertial effects of the gas motion, conservation of momentum requires the pressure to be continuous:

$$\hat{P}_g^b = \hat{P}_g^u, \tag{5}$$

Finally, we consider an energy balance. The heat liberated by the reaction is used to heat the two phases to the adiabatic combustion temperature (a fraction of this energy is passed forward into the preheat zone). In treating the jump in energy across the reaction/preheat zone, the gas in the product region is at the adiabatic flame temperature and the gas flowing ahead of this "jump" is equilibrated to the cool unreacted temperature:

$$\hat{\rho}_g^u \hat{v}_g^u (\hat{e}_g^u + \frac{\hat{P}_g}{\hat{\rho}_g^u}) = \hat{V}_F(\hat{\rho}_s^u \hat{e}_s^u + \hat{\rho}_g^u \hat{e}_g^u - \hat{\rho}_s^b \hat{e}_s^b - \hat{\rho}_g^b \hat{e}_g^b), \tag{6}$$

where $\hat{e}_i$ is the internal energy of each phase, including the heat of formation.

The ideal gas law is then used to relate the pressure, density and temperature of the gas phase. As a simplification in the present model, we assume that the reacted region is at a constant adiabatic flame temperature and the unreacted material is at a known uniform low temperature. (The reader should refer to Appendix B for the details and implications of this approximation.) Therefore, on either side of the combustion front:

$$\hat{\rho}_g^u = \frac{\phi_g^u \hat{P}^\circ}{\hat{R}\hat{T}^\infty}; \qquad \hat{\rho}_g^b = \frac{\phi_g^b \hat{P}^\circ}{\hat{R}\hat{T}^\circ}; \tag{7}$$

where, $\hat{P}^\circ$ is the pressure at the burn front, $\hat{T}^\circ$ is the adiabatic flame temperature, $\hat{T}^\infty$ is the ambient temperature of the unreacted material,and $\hat{R}$ is the gas constant for the gaseous combustion products .

Porosities, ϕ_g^u and ϕ_g^b , are determined by the solid volume fraction in each region according to a saturation volume constraint:

$$\phi_g + \phi_s = 1. \tag{8}$$

The mass conservation jump relationship can be then rewritten as:

$$\frac{\phi_g^u \hat{P}^\circ}{\hat{R}\hat{T}^\infty} \hat{v}_g^u = \hat{V}_F(\hat{\rho}_s^u - \hat{\rho}_s^b) + \hat{V}_F \frac{\phi_g^u \hat{P}^\circ}{\hat{R}\hat{T}^\infty}(1 - \frac{\phi_g^b \hat{T}^\infty}{\phi_g^u \hat{T}^\circ}). \tag{9}$$

In addition, we consider the mass generation of gas, $\hat{V}_F(\hat{\rho}_s^u - \hat{\rho}_s^b)$, to be constant. Note that this restriction can be removed and the case of variable burn velocity and/or variable solid volume fraction changes can be treated.

Balance Equations for Regions Exterior to the Flame Zone

As described above, the reacted porous medium is treated as being highly permeable and only a temporal variation of pressure is considered in this region. The thermodynamic state of the gas is determined solely by the pressure generated at the flame front and the gas-solid temperature (fixed at the adiabatic flame temperature).

In the unreacted region, $\hat{x} > \hat{V}_F\hat{t}$, the laminar gas flow equations are:

$$\frac{\partial\hat{\rho}_g}{\partial\hat{t}} + \frac{\partial(\hat{\rho}_g v_g)}{\partial\hat{x}} = 0, \tag{10}$$

$$\hat{v} = -\frac{\hat{\kappa}}{\phi_g^u\hat{\mu}_g}\frac{\partial\hat{P}_g}{\partial\hat{x}}; \tag{11}$$

where $\hat{\kappa}$ is the permeability of the unreacted medium and $\hat{\mu}_g$ is the gas molecular viscosity. The spatial and time coordinates are denoted by the variables $\hat{x}$ and $\hat{t}$, respectively.

In the reacted region, $\hat{x} < \hat{V}_F\hat{t}$, the governing equations are:

$$\hat{T}_g = \hat{T}^\infty = constant, \tag{12}$$

$$\phi_g^b\hat{P}_g = \hat{\rho}_g\hat{R}\hat{T}_g. \tag{13}$$

Next, we introduce the following nondimensionalization scheme to describe one-dimensional combustion wave propagation within a fixed bed length, $\hat{L}$:

$$\begin{aligned} P &= \frac{\hat{P}}{\hat{P}_{ref}}; & x &= \frac{\hat{x}}{\hat{L}}; & t &= \frac{\hat{t}\hat{V}_F}{\hat{L}}; \\ \lambda &= (1 - \frac{\phi_g^b\hat{T}^\circ}{\phi_g^u\hat{T}^\infty}); & \kappa &= \frac{\hat{\kappa}\hat{P}_{ref}}{\phi_g^u\hat{\mu}_g\hat{V}_F\hat{L}}; & \hat{P}_{ref} &= (\hat{\rho}_s^u - \hat{\rho}_s^b)\frac{\hat{R}\hat{T}^\infty}{\phi_g^u}. \end{aligned} \tag{14}$$

In the reacted region, $x < t$, the gas pressure is spatially uniform at the pressure of the burn front, P° , and in the unreacted region, $x > t$, the gas flow is related to the pressure gradient according to the Darcy approximation. Combining equations 10 and 11 with the ideal gas law produces the following description of the pressure field:

$$\frac{\partial P}{\partial t} = \kappa \frac{\partial}{\partial x}(P \frac{\partial P}{\partial x}). \tag{15}$$

The gas initially within the reactor is at ambient pressure, P^{∞}.

The balance of mass at $x = t$ requires:

$$-\kappa P \frac{\partial P}{\partial x} = 1 + \lambda P. \tag{16}$$

and the boundary constraint on gas pressure at $x = 1$ is:

$$P = P^{\infty}. \tag{17}$$

Note that the exit boundary condition can easily be modified to include a variable back-pressure condition. Such a constraint might be needed to model the pressure gradient imposed by a frit endplate at the bed exit. The exit mass flow rate (at $x = 1$) , denoted $\dot{m}$, is defined as:

$$\dot{m} = \frac{\hat{\rho}_g \hat{v}_g}{\hat{V}_F(\hat{\rho}_s^u - \hat{\rho}_s^b)}. \tag{18}$$

We see that our model reduces to a nonlinear, parabolic differential equation with an interface condition which traverses the reactor at $x = t$. Solutions to this model are a function of only two nondimensional parameters, λ and κ, which are related to the thermodynamics of the combustion process and the permeability of the unreacted porous material.

4 Numerical Method

In obtaining numerical solutions of equation 15, we found it very convenient to introduce a coordinate transformation which maps the computational domain

domain to a fixed interval. The location of the flame front is mapped to the origin and the bed exit is given a coordinate of one with the following variable changes:

$$\xi = \frac{(x-t)}{(1-t)}; \qquad \tau = t. \tag{19}$$

This yields a transformed equation:

$$\frac{\partial P}{\partial \tau} + \frac{(\xi-1)}{(1-\tau)}\frac{\partial P}{\partial \xi} = \frac{\kappa}{(1-\tau)^2}\frac{\partial}{\partial \xi}(P\frac{\partial P}{\partial \xi}). \tag{20}$$

The burn front constraint at $\xi = 0$ becomes:

$$-\frac{\kappa}{(1-\tau)}P\frac{\partial P}{\partial \xi} = 1 + \lambda P, \tag{21}$$

and at $\tau = 0$ and $\xi = 1$: $\qquad P = P^{\infty}$.

Numerical solutions of equation (20) were obtained using a method-of-lines algorithm with 4th-order spatial differences on a computational grid of twenty-one nodes and an Adams-Moulton implicit time-integration scheme [12]. Typical computations for complete combustion of a model reactor require 100 seconds (actual cpu time) on a CDC 6600.

5 Results

For demonstration purposes, the following dimensional variables were chosen for a representative reactor of length $\hat{L} = 3\ cm$:

$$\begin{aligned} \phi_g^b &= 0.5; \qquad \hat{T}^{\circ} = 1500°\mathrm{K}; \qquad \hat{V}_F = 2\ cm/s; \\ \phi_g^u &= 0.3; \qquad \hat{T}^{\infty} = 300°\mathrm{K}; \qquad \hat{\Gamma}_s = 2\ g/cm^3. \end{aligned} \tag{22}$$

The dimensional permeability of the unreacted porous medium is estimated using the Blake-Kozney formula [10]:

$$\hat{\kappa} = \frac{\phi_g^3 \hat{d}_p^2}{150(1-\phi_g)^2}. \tag{23}$$

As a representative gas viscosity we used $\hat{\mu}_g = 2.0 \times 10^{-4}\ gm/cm \cdot s$ and the reactant is assumed to be composed of uniform particles 1 μm in diameter. The resulting reference permeability and pressure are:

$$\hat{\kappa} = 3.6 \times 10^{-12}\ cm^2; \qquad \hat{P}_{ref} = 1.1 \times 10^{10}\ dyne/cm^2.$$

The nondimensional parameters λ and κ are 0.67 and 30.0, respectively. Results are given below for cases with these parameters and two lower values of κ , 0.5 and 2.0.

Figures 4 to 6 show the spatial pressure profiles at selected times during combustion for the cases described above. Ignition of the porous bed occurs at $t = 0$ and $t = 1$ corresponds to the completion of burning. The choice of a normalized pressure-squared ordinate in these plots is to facilitate comparison with analytical solutions described below. Note that at early times, the gas permeates only a short distance in front of the flame and there is no flow ahead of this layer.

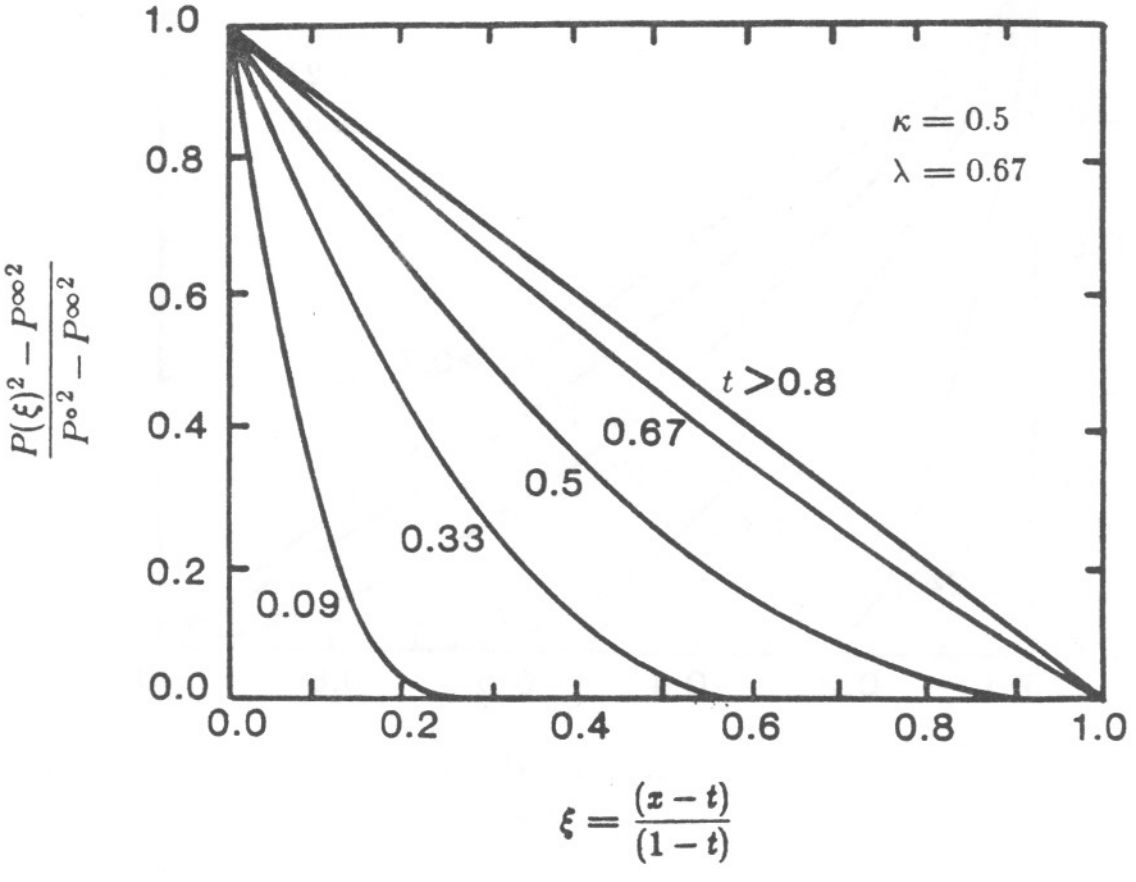

Figure 4. Temporal variation of the pressure-squared profile for model parameters κ =0.5 and λ =0.67 .

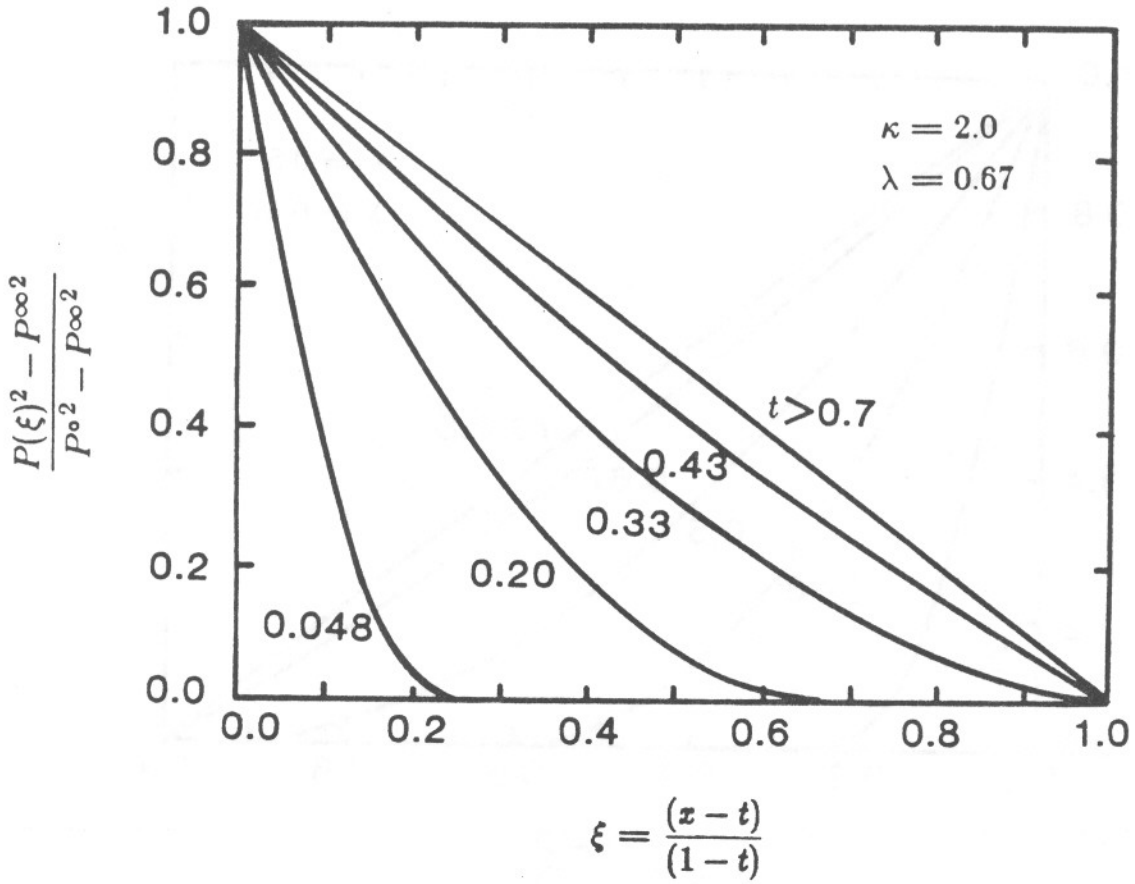

Figure 5. Temporal variation of the pressure-squared profile for model parameters κ =2.0 and λ =0.67 .

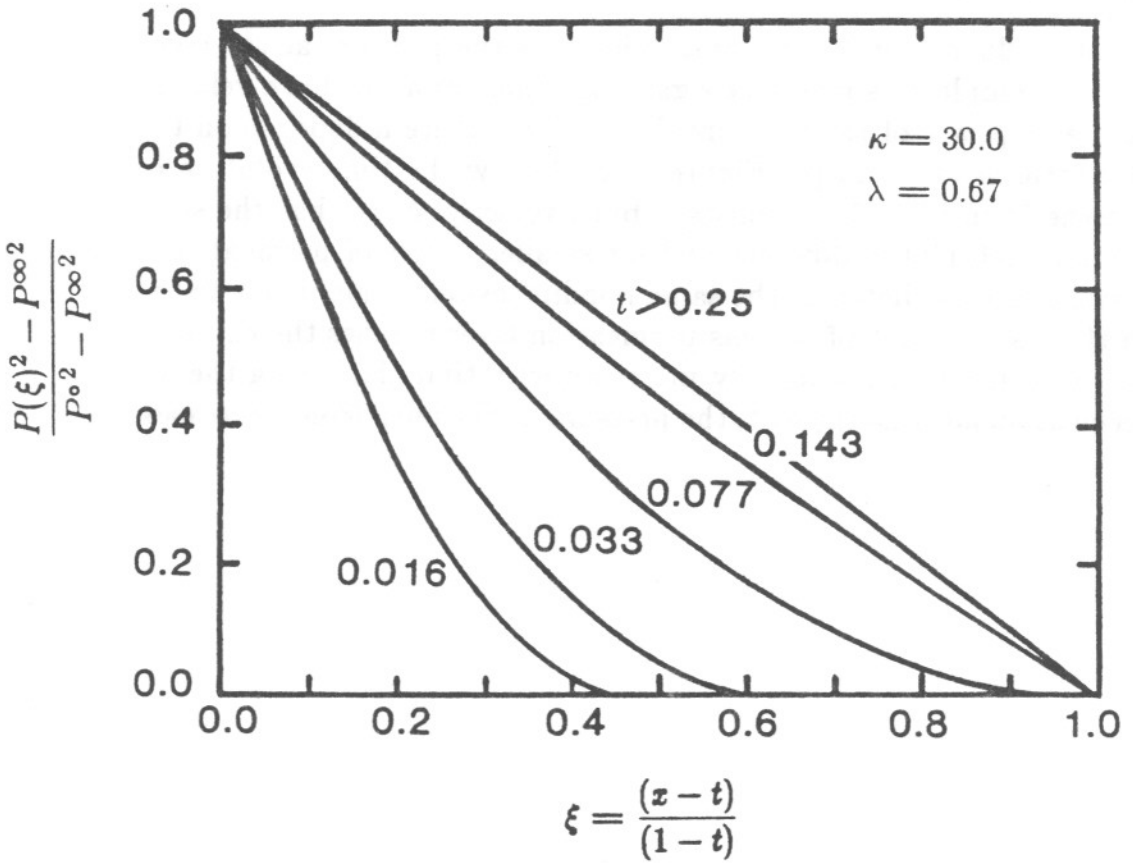

Figure 6. Temporal variation of the pressure-squared profile for model parameters κ =30.0 and λ =0.67 .

With increasing time, the leading edge of the permeation layer reaches the open, unconstrained end of the reactor and very rapidly a quasi-steady gas flow is established between the combustion wave and the exit. This quasi-steady flow is characterized by a pressure profile which varies with the square root of distance. As the nondimensional permeability increases, the steady-state flow is reached at earlier times. In an unstretched coordinate system that moves with the flame, the pressure in the permeation layer decreases approximately linearly with distance in front of the combustion front.

An important influence on the burning velocity is the pressure at the combustion front. For example, in single-phase gaseous combustion the burn velocity is found to vary as a power of the pressure: $V_F \sim P^n$, where n depends on the details of the kinetic mechanism [7]. Figures 7 to 9 show the time evolution of the pressure at the burn front for a constant burn velocity. Note that the scale of the ordinate for each plot is different and for smaller values of permeability, κ , higher pressures are predicted at the same nondimensional time. Prior to the time at which the leading edge of the gas permeation layer reaches the exit, the pressure at the burn front monotonically increases with time. Following the arrival of the permeation layer at the exit, the pressure at the burn front decreases.

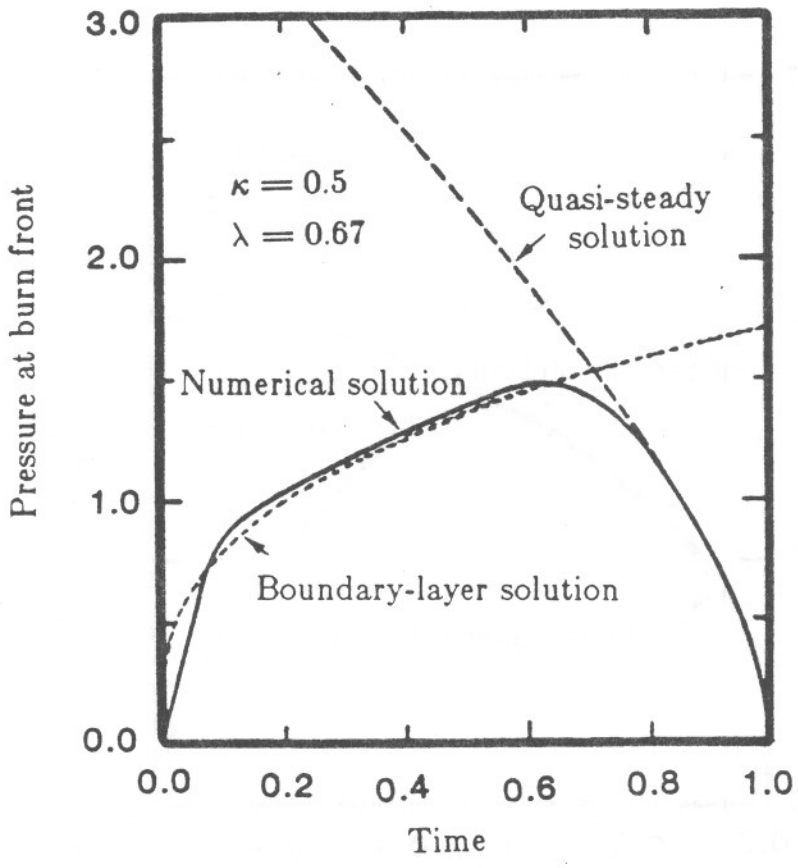

Figure 7. Temporal variation of the nondimensional burn front pressure for the parameters $\kappa = 0.5$ and $\lambda = 0.67$.

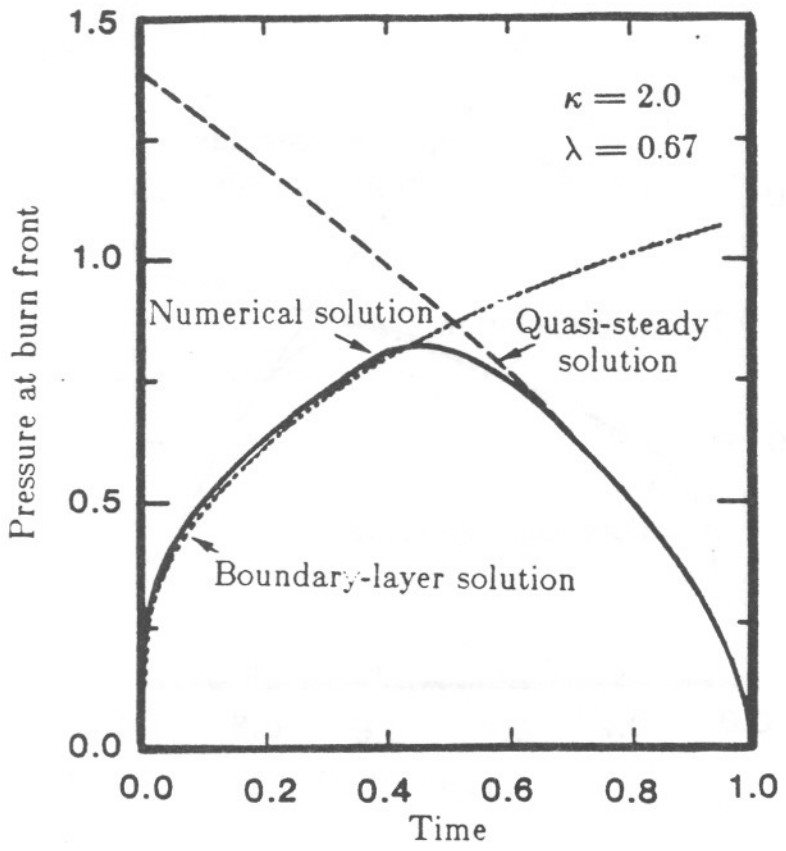

Figure 8. Temporal variation of the nondimensional burn front pressure for the parameters $\kappa = 2.0$ and $\lambda = 0.67$.

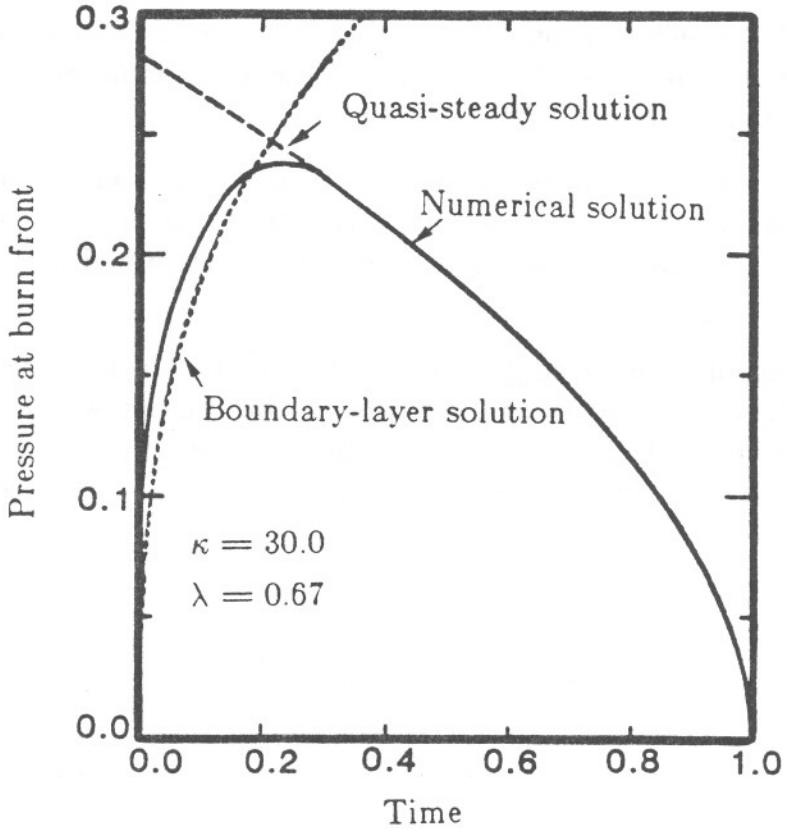

Figure 9. Temporal variation of the nondimensional burn front pressure for the parameters κ =30. and λ =0.67 .

Pressure development prior to the gas venting occurs in two stages. This can be seen in Figure 7 for the case of a nondimensional permeability, κ =0.5. The initial stage corresponds to the growth of a boundary layer ahead of the flame. Upon reaching a steady state (in a moving coordinate attached to the flame), the pressure at the burn front increases toward an asymptotic value of P°_{max}:

$$P^{\circ}_{max} = \frac{(1+P^{\infty})}{(1-\lambda)}.$$

This asymptotic value of pressure can only be reached in a porous bed with a very small nondimensional permeability. In the present case, the nondimensional asymptotic overpressure has a value of 3.03.

After the gas permeation layer reaches the exit, the gas flow quickly adjusts to a quasi-steady rate determined only by the combustion front gas pressure and the distance to the exit. An analytic solution has also been determined for this flow.

The temporal variation of normalized gas mass outflow, $\dot{m}$, is shown in Figure 10. Note that there is effectively zero mass flow prior to the time at which the permeation layer reaches the exit. For a very large permeability the gas mass outflow is constant, *i.e.* , $\dot{m} = 1$ during the entire burn.

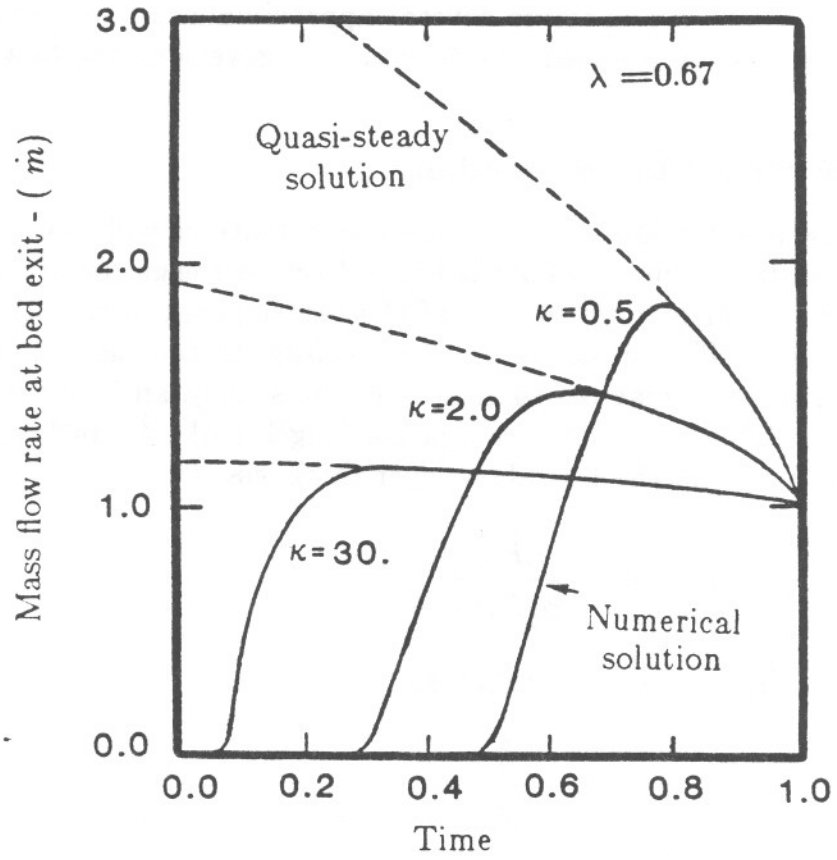

Figure 10. Nondimensional mass flow at the bed exit as a function of time.

6 Analytical Solutions

For the two extremes of low and high permeability ($\kappa \to 0$ and $\kappa \to \infty$, respectively) analytical solutions to the flow equations have been determined. In the subsections to follow, we examine several approximate techniques and alternative methods for solving the basic model equation governing the flow.

Gas Permeation Boundary Layer Solution

In the limit of low permeability, $\kappa \to 0$, the exit conditions will have little effect on the pressure distribution ahead of the flame. Because the gas permeation layer is so thin, the flow will be independent of the venting condition until the flame front nears the exit. This situation can be idealized to the case of flame propagation in a semi-infinite reactor. In this case, the scaling and coordinate transformations are modified to remove the reactor length scale, $\hat{L}$, in favor of an alternative scaling based on the boundary layer thickness, $\hat{\delta}$:

$$\hat{\delta} = \frac{\hat{\kappa}\hat{P}_{ref}}{\phi_g^u \hat{\mu}_g \hat{V}_F} \tag{24}$$

Similarly, the relevant time scale, $\hat{\tau}$, is taken as:

$$\hat{\tau} = \frac{\hat{\delta}}{\hat{V}_F}, \tag{25}$$

and we retain the reference pressure, $\hat{P}_{ref}$, defined previously.

In order to follow the boundary layer development ahead of the flame, we introduce a wave coordinate which travels with the flame velocity and has its origin at the flame. In these coordinates, the governing nondimensional equation is given as:

$$\frac{\partial P}{\partial \tau} - \frac{\partial P}{\partial \eta} = \frac{\partial}{\partial \eta}(P\frac{\partial P}{\partial \eta}), \tag{26}$$

and the boundary condition is

$$-P^\circ \frac{\partial P^\circ}{\partial \eta} = 1 + \lambda P^\circ, \tag{27}$$

where:

$$\eta = \frac{\hat{x} - \hat{V}_F \hat{t}}{\hat{\delta}} \quad , \tau = \frac{\hat{t}}{\hat{\tau}} \quad and \quad P = \frac{\hat{P}}{\hat{P}_{ref}}.$$

Note that with this coordinate scaling, only one parameter, λ, determines the character of the solution of equation (26).

Equation (26) has been solved numerically for the case $\lambda = 0.67$. The temporal variation of the normalized pressure at the flame front is shown in Figure 11 and the spatial distribution of the pressure in the boundary layer is shown in Figure 12. Note that a linear variation of pressure with distance ahead of the flame is predicted. This observation is the basis for an approximate integral solution method which is described below.

From Figure 12, it is seen that the pressure has reached 94% of it's final value at a nondimensional time of 8. Examinination of the pressure profiles at later times indicates that they are practically indistinguishable. This suggests that the solution approaches a steady state relative to the moving coordinate system. By setting the time derivative of equation (26) to zero, the steady-state profile is obtained. A single integration of the resulting equation produces:

$$P + P\frac{\partial P}{\partial \eta} = constant. \tag{28}$$

Far upstream, the pressure must drop to an ambient level and the pressure gradient must vanish. Using these boundary conditions, the constant can be evaluated to obtain:

$$P + P\frac{\partial P}{\partial \eta} = P^{\infty}. \tag{29}$$

The conservation of mass across the burn front determines the overpressure generated by the combustion and the maximum pressure developed in this steady-state solution is given as:

$$P^{\circ}_{max} = \frac{(1 + P^{\infty})}{(1 - \lambda)}. \tag{30}$$

The boundary layer profile has a particularly simple form in the limiting case where the pressure at the flame front greatly exceeds the ambient value. If

we set $P^\infty = 0$ the solution of equation (29) is:

$$\begin{aligned} P &= P^\circ_{max} - \eta \qquad P^\circ_{max} \geq \eta \geq 0, \\ P &= 0 \qquad\qquad\qquad \eta \geq P^\circ_{max} \end{aligned} \tag{31}$$

Note that there is a discontinuity in slope at the leading edge of the permeation layer ($\eta = P^\circ_{max}$) which is due to the approximation that the ambient pressure is zero.

An exact solution to the boundary layer equation (Eq. 29) has been determined and the solution can be expressed in terms of the following normalized variables:

$$\begin{aligned} \psi &= \frac{(P - P^\infty)}{(P^\circ_{max} - P^\infty)} \\ \theta &= \frac{\eta}{(P^\circ_{max} - P^\infty)}, \end{aligned} \tag{32}$$

and a single parameter, ϵ, which is the ratio of ambient pressure to the overpressure induced by combustion:

$$\epsilon = \frac{P^\infty}{(P^\circ_{max} - P^\infty)}. \tag{33}$$

Thus, equation (29) is transformed to:

$$\psi + (\psi + \epsilon)\frac{d\psi}{d\theta} = 0. \tag{34}$$

Boundary conditions are $\psi = 1$ at $\theta = 0$ and $\psi \to 0$ as $\theta \to \infty$. A direct integration of the differential equation produces the following transcendental solution:

$$\psi + \epsilon \ln \psi = 1 - \theta. \tag{35}$$

The structure of the pressure wave solution is more clearly illustrated by asymptotic expansions (for small ϵ) in the regions: A - near the flame front for $\theta \ll 1$; B - near the foot of the pressure wave at $\theta \approx 1$; C - in the outer region of the boundary layer for $\theta \gg 1$. These approximate solutions are:

Region A ($\theta \ll 1$)

$$\psi \sim 1 - \theta - \epsilon \ln(1 - \theta), \tag{36}$$

Region B ($\theta \approx 1$)

$$\psi \sim 1 - \theta - \epsilon \ln \epsilon, \tag{37}$$

Region C ($\theta \gg 1$)

$$\psi \sim \exp(\frac{1-\theta}{\epsilon}). \tag{38}$$

The singular character of the solution dependence on ϵ is clearly brought out by these expansions. A discussion of the mathematical details of this general type of wave structure can be found in Reference 13.

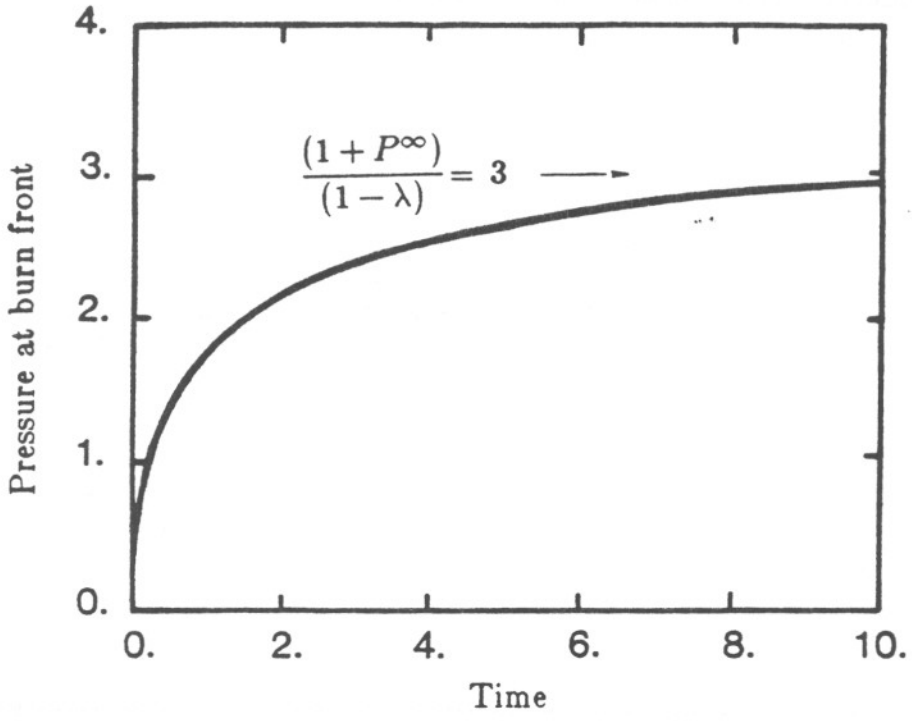

Figure 11. Time variation of normalized pressure at burn front for $\lambda = 0.67$

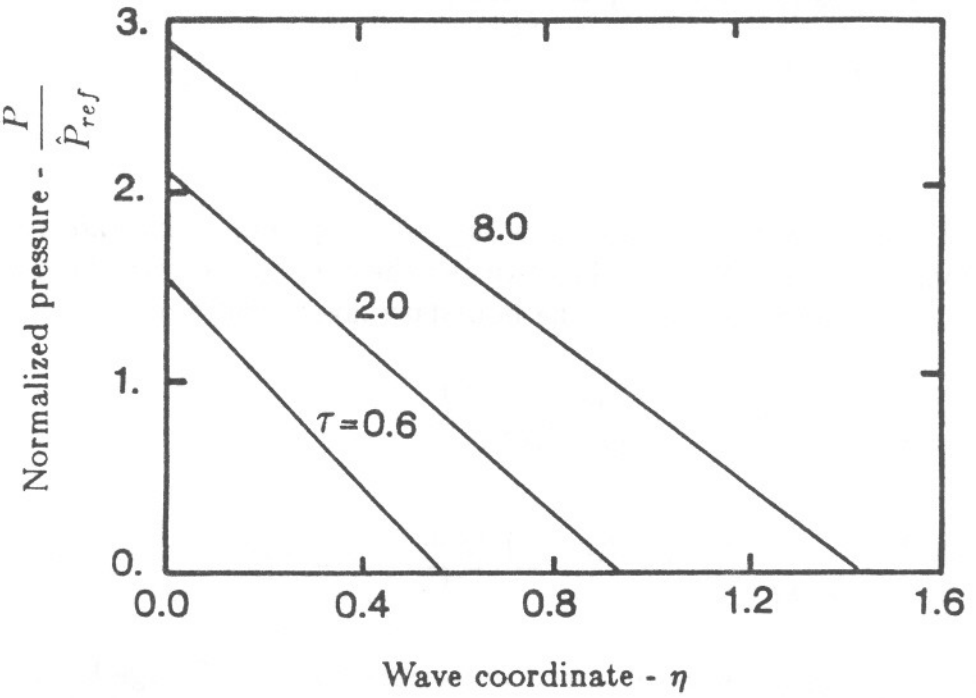

Figure 12. Spatial distribution of pressure in the boundary layer for $\lambda = 0.67$

Integral Boundary-layer Solutions

The simple form of the boundary-layer pressure variations determined in the previous section can be utilized to develop an integral solution method which reduces the transient problem to solving an ordinary differential equation. We assume that the boundary layer has a time-dependent thickness, $\delta(t)$, and the variation of pressure within the boundary layer can be approximated as:

$$\begin{aligned} P &= P^{\circ}(t) && x < t, \\ (P - P^{\infty}) &= (P^{\circ} - P^{\infty})(1 - \frac{(x-t)}{\delta(t)}) && t < x < \delta, \\ P &= P^{\infty} && x > \delta. \end{aligned} \tag{39}$$

This form of the pressure variation was suggested by numerical and approximate solutions valid for $P^{\infty} \sim 0$. Substituting these equations into the gas pressure equation and integrating across the boundary layer results in:

$$\delta(t) = \frac{\kappa P^{\circ}(P^{\circ} - P^{\infty})}{(1 + \lambda P^{\circ})},$$

$$\frac{d}{dt}(\frac{P^{\circ}(P^{\circ} - P^{\infty})^2}{(1 + \lambda P^{\circ})}) = \frac{2(1-\lambda)}{\kappa}(\frac{(1 + P^{\infty})}{(1-\lambda)} - P^{\circ}). \tag{40}$$

Solutions to this equation were obtained numerically using a Runge-Kutta-Fehlberg method [14]. Predictions with this model for the case of $\lambda = 0.67$ are superimposed on Figures 7 to 9 as broken curves. Clearly, the early-time growth of pressure is accurately approximated by the integral method. However, at later time, venting of the permeated gas occurs and a different pressure development occurs. The next section describes an analytical solution which incorporates the venting of the product gases.

Quasi-steady Solution

After the leading edge of the gas permeation layer reaches the reactor exit, the flow can be approximated as though there was a steady flow of gas from the burn front to the bed exit at any given time. The flowrate will vary as the driving pressure in the burned region changes with time. This mode of gas transfer is particularly relevant to reactants which are highly permeable. By setting the time

derivative in the transformed equation (20) equal to zero a quasi-steady solution is obtained. The resulting ordinary differential equations can be integrated to yield:

$$(P^2 - P^{\infty 2}) = (P^{\circ 2} - P^{\infty 2})(1 - \frac{(x-t)}{(1-t)}), \tag{41}$$

where the pressure at the burn front, P°, is determined by:

$$P^\circ = \frac{\lambda(1-t)}{\kappa} + (\frac{\lambda^2(1-t)^2}{\kappa^2} + P^{\infty 2} + \frac{2(1-t)}{\kappa})^{\frac{1}{2}}. \tag{42}$$

The mass flux of combustion-product gas at $x = 1$ is:

$$\dot{m} = (1 + \lambda P^\circ). \tag{43}$$

In Figures 4 to 10, the two analytical solutions have been plotted along with the results of the numerical calculations. As seen in these figures, after the gas flow reaches the bed exit, the pressure quickly changes to one consistent with the quasi-steady solution even for low and intermediate values of permeability, κ.

An approximate but complete analytical model of the pressure field in the reactor is obtained by using the boundary layer model of the previous section at early times and the quasi-steady model at later times. Overlaying the temporal variation of burn front pressure predicted by these solutions produces curves which intersect at a particular time. This is the time when the leading edge of the gas permeation layer has reached the bed exit.

7 Summary

With the use of a simple model it has been shown that internal gas flow and pressure induced by combustion can be estimated without considering the detailed structure of the reaction zone. Our model treats the combustion wave as a density/temperature discontinuity which propagates at a known burn velocity. The burn velocity must be determined separately by either experiment or a detailed kinetic model of the reaction zone.

The utility of our basic model is in the use of the thin flame approximation. Several additional restrictions are imposed to demonstrate results for a particular reactive system. These restrictions can be easily modified to obtain more realistic models. High Reynolds number gas flows can be calculated by including the appropiate inertial corrections to the permeation law [15]. Appendix C examines an approach for treating this modification. In addition, the model can be extended to treat pressure gradients in the reacted region or gasdynamic flows in the case of complete gasification of the reactant as outlined in Appendix D. Other simple variations could include a variable burn velocity and the one-dimensional propagation through a variable corss-sectional area reactor.

Our calculations show that the development of the pressure field has a strong dependence on the permeability of the reactants. Any physical process which can modify the permeability during the combustion, such as the presence of a melt phase or a compaction front, should be considered in more detailed models.

8 References

1. **Sivashinsky, G.I.**
   Hydrodynamic Theory of Flame Propagation in an Enclosed Volume ,*Acta Astronautica* **6** ; 631,1979.
2. **Bradley, D. and Mitchenson, A.**
   Mathematical Solutions for Explosions in Spherical Vessels ,*Combustion and Flame* **26** ; 201, 1976.
3. **Buckmaster, J.D. and Ludford, G.S.S.**
   Theory of Laminar Flames ,Cambridge University Press, 1982.
4. **Margolis, S.B. and Green, R.M.**
   Theoretical Prediction of Self-Propagating, Diffusion- and Decomposition-Limited Intermetallic Reactions ;*Sandia National Labs.*, SAND78-8502, 1978.
5. **Kuo, K. and Summerfield, M.**
   High Speed Combustion of Mobile Granular Solid Propellant: Wave Structure and the Equivalent Rankine-Hugoniot Relation ,*15th Symposium (International) on Combustion* ; 515, 1974.
6. **Bernecker, R.R., Sandusky, H.W.,and Clairmont, A.R.**
   Deflagration-to-Detonation Transition Studies of Porous Charges in Plastic Tubes, *Seventh Symposium (International) on Detonation ;* 119, 1981.
7. **Strehlow, R.A.**
   Fundamentals of Combustion ,International Textbook, Scranton, Pa., 1968.
8. **Schumann, T.E.W.**
   Heat Transfer of a Liquid Flowing Through a Porous Prism ,*J. Franklin Inst.*, **28** ; 405, 1929.
9. **Denton, W.**
   The Heat Transfer and Flow Resistance for Fluid Flow Through Randomly Packed Spheres ,*ASME Transactions* ; 370, 1951.
10. **Bird, B.R., Stewart, W.E., and Lightfoot, E.N.**
    Transport Phenomena ,John Wiley and Sons, 199, 1960.
11. **Shepherd, J.E. and Begeal, D.**
    Transient Compressible Flow in Porous Materials ,*Sandia National Labs.*, SAND83-1788, 1983.
12. **Hyman, J.M.**
    The Method of Lines Solution of Partial Differential Equations ,*Courant Institute of Mathematical Sciences,* COO-3077-139, 1976.
13. **O'Malley, R.E. Jr.**
    On Singular Perturbations Problems with Interior Nonuniformities ,*J. Math. Mech.*, **19** ,1103, 1970.

14. Shampine, L.F. and Watts, H.A.
DEPAC- Design of a User Oriented Package of ODE Solvers ,*Sandia National Labs.*, SAND79-2374, 1979.

15. Dullien, F.A.L.
Porous Media Fluid Transport and Pore Structure ,Academic Press, 1979.

9 Appendix A

Thermal Nonequilibrium in the Preheat Zone

In this appendix, we examine the thermal structure of the preheat zone ahead of a combustion wave. Our formulation of the thermal field follows a model first examined by Schumann [8].

Consider a combustion wave discontinuity which propagates at a constant velocity, $\hat{V}_F$, and generates combustion gas at $\hat{x} = \hat{V}_F \hat{t}$. We assume the porous material is packed into a rigid bed and that the only exchange of energy between the solid- and gas-phase is due to interphase convective heat transfer. The resulting equations governing the flow are as follows:

conservation of gas mass,

$$\frac{\partial \hat{\rho}_g}{\partial \hat{t}} + \frac{\partial}{\partial \hat{x}}(\hat{\rho}_g \hat{v}_g) = 0; \tag{1A}$$

conservation of momentum of the gas phase (Darcy's law),

$$\hat{v}_g = -\frac{\hat{\kappa}}{\phi_g \hat{\mu}_g} \frac{\partial \hat{P}_g}{\partial \hat{x}}; \tag{2A}$$

conservation of gas- and solid-phase energies,

$$\frac{\partial}{\partial \hat{t}}(\hat{\rho}_g \hat{T}_g) + \frac{\partial}{\partial \hat{x}}(\hat{\rho}_g \hat{v}_g \hat{T}_g) = \frac{\hat{\mathcal{H}}}{\hat{c}_g}(\hat{T}_s - \hat{T}_g), \tag{3A}$$

$$\frac{\partial \hat{T}_s}{\partial \hat{t}} = -\frac{\hat{\mathcal{H}}}{\hat{\rho}_s \hat{c}_s}(\hat{T}_s - \hat{T}_g) + \hat{\alpha}_s \frac{\partial^2 \hat{T}_s}{\partial \hat{x}^2}; \tag{4A}$$

and the equation of state of the gas (ideal gas),

$$\phi_g \hat{P} = \hat{\rho}_g \hat{R} \hat{T}_g. \tag{5A}$$

The nomenclature is the same as that used in the main text. The interphase heat transfer coefficient, $\hat{\mathcal{H}}$, is estimated using an empirical relationship taken from the packed bed literature [9]:

$$\hat{\mathcal{H}} = \frac{12(1-\phi_g)\hat{k}_g}{\hat{d}_p^2}, \tag{6A}$$

where, $\hat{k}_g$ is the gas thermal conductivity and $\hat{d}_p$ is the surface mean particle size of the porous reactant.

In addition to the nondimensional variables used in the main text, we introduce the following nondimensional parameters:

$$\beta = \frac{\hat{\mathcal{H}}\hat{\kappa}\hat{R}\hat{T}^{\infty}}{\hat{c}_g\phi_g\hat{\mu}_g\hat{V}_F^2}; \qquad \epsilon = \frac{\hat{c}_g\hat{R}\hat{T}^{\infty}}{\hat{c}_s\hat{P} - ref\phi_g\hat{\rho}_s^u}; \qquad \alpha = \frac{\hat{\alpha}_s\hat{\mu}_g}{\hat{\kappa}\hat{P}_{ref}}. \tag{7A}$$

The nondimensional quantity, ϵ , is the ratio of thermal capacitance of the gas to the solid; α is a nondimensional thermal diffusivity of the solid reactant and β is the ratio of interphase convective heat transfer to the rate at which heat is advected by the hot combustion gases. Granular materials composed of small particles have a very large surface area which is available for heat transfer and we expect β to be a large quantity. For the representative reactor variables given in the main text, we estimate that $\alpha \sim \epsilon \sim 10^{-2}$ and $\beta \sim 10^{7}$.

In order to obtain more quantitative estimates of the thermal boundary layer thickness, we will examine the structure of a steady preheat zone. First, the conservation equations are transformed to a coordinate system which moves with the combustion wave. Setting the time derivatives to zero yields the following equations in terms of a steady wave coordinate, $\eta = x - t$:

$$\frac{d}{d\eta}(\rho_g v_g - \rho_g) = 0, \tag{8A}$$

$$v_g = -\frac{dP}{d\eta}, \tag{9A}$$

$$\frac{d}{d\eta}(\rho_g v_g T_g - \rho_g T_g) = \beta(T_s - T_g), \tag{10A}$$

$$\frac{dT_s}{d\eta} + \alpha \frac{d^2T_s}{d\eta^2} = \epsilon\beta(T_s - T_g), \tag{11A}$$

$$P = \rho_g T_g. \tag{12A}$$

The rate of gas generation by the combustion, σ , is defined by integration of equation (8A):

$$\rho_g v_g - \rho_g = \sigma. \tag{13A}$$

Note that σ is a positive quantity ($\hat{v}_g > \hat{V}_F$), and has a value of order one.

The convective heat transfer between the gas and the solid can be eliminated by combining equations (10A) and (11A) to obtain:

$$\epsilon\sigma \frac{dT_g}{d\eta} = \frac{dT_s}{d\eta} + \alpha \frac{d^2T_s}{d\eta^2}. \tag{14A}$$

Integrating this equation once with respect to η yields:

$$\epsilon\sigma(T_g - T^\infty) = (T_s - T^\infty) + \alpha \frac{d}{d\eta}(T_s - T^\infty). \tag{15A}$$

In order to evaluate the constants of integration, we use the conditions $T_g \to T^\infty$, $T_s \to T^\infty$, and $\frac{d}{d\eta}(T_s - T^\infty) \to 0$, in the cold reactant far ahead of the combustion wave ($\eta \to \infty$).

With this relationship, the gas-phase temperatures can be eliminated in equation 11A, and the solid reactant temperature is governed by the following ordinary differential equation:

$$\frac{d^2T_s}{d\eta^2} + \frac{(\sigma + \beta\alpha)}{\alpha\sigma} \frac{dT_s}{d\eta} + \frac{\beta(1 - \epsilon\sigma)}{\alpha\sigma}(T_s - T^\infty) = 0, \tag{16A}$$

which for large β has the solution

$$T_s - T^\infty = c_1 \exp\left(-\frac{\beta\eta}{\sigma}\right) + c_2 \exp\left(-\frac{(1 - \epsilon\sigma)\eta}{4\alpha}\right). \tag{17A}$$

From equation (15A) it follows that the gas-phase temperature has similar exponential behavior. The constants c_1 and c_2 are determined by requiring

that $T_s \to T_{ign}$ (reactant ignition temperature) and $T_g \to T^\circ$ (adiabatic flame temperature) at the flame front $\eta \to 0$. From the exponential nature of equation (17A), it is clear that the preheat zone is composed of two boundary layer regions. Close to the flame is a region where convective heat transfer dominates the heat transfer. The length of this region is of the order $\delta_{convection} \sim \frac{1}{\beta}$. The outer region is dominated by the effect of thermal conduction. As expected, the conduction dominated region has a length of the order $\delta_{conduction} \sim \alpha$. For reactant beds with large specific surface area (*i.e.* small particles) the region of solid-gas nonequilibrium is small – well within the preheat limit as determined by conduction alone. Pictorially, the temperature distributions given by the above analysis are as shown in the figure below.

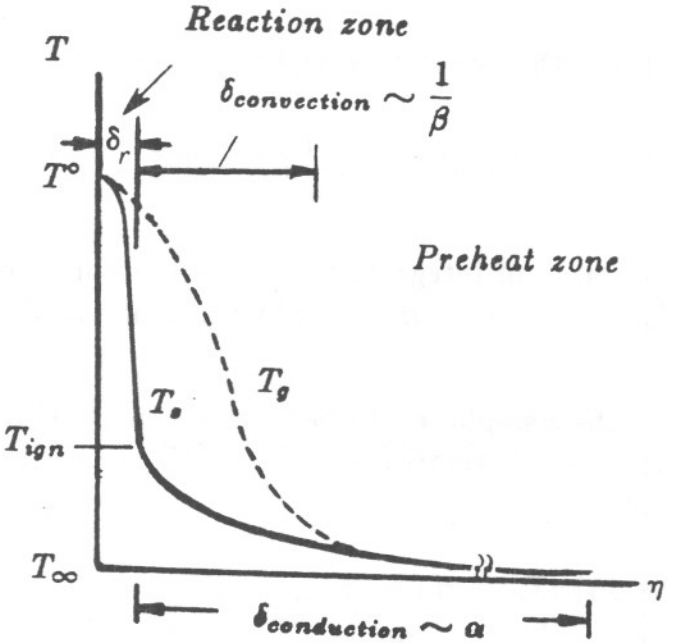

Figure 13. Solid- and gas-phase temperatures in the preheat zone.

10 Appendix B

Temperature Field in Reacted Region

In this appendix, we examine the energy jump condition given in the main text. This jump condition is used to provide a definition of the adiabatic flame temperature of the fully reacted region. We shall show that the assumption of an isothermal temperature of the reacted region is valid when the solid phase, fully reacted material is in thermal equilibrium with the combustion-product gases. By definition, the internal energy of the solid and gas phases are:

$$\hat{e}_g = \hat{e}_g^{\mathcal{F}} + \hat{c}_g(\hat{T} - \hat{T}^{\infty}), \tag{1B}$$

$$\hat{e}_s = \hat{e}_s^{\mathcal{F}} + \hat{c}_s(\hat{T} - \hat{T}^{\infty}); \tag{2B}$$

where $\hat{e}_g^{\mathcal{F}}$ and $\hat{e}_s^{\mathcal{F}}$ are the heats of formation at T^{∞} and $\hat{c}_g$ and $\hat{c}_s$ are the specific heats of the gas and solid phases.

Combining equations (4) and (6) of the main text with the above definitions of internal energy, produces the following energy balance:

$$(\hat{\rho}_s^u - \hat{\rho}_s^b)(\hat{e}_g^{\mathcal{F}} - \hat{e}_s^{\mathcal{F}}) + ((\hat{\rho}_g^u - \hat{\rho}_g^b) + (\hat{\rho}_s^u - \hat{\rho}_s^b))\frac{\hat{P}}{\hat{\rho}_g^u} = -(\hat{\rho}_s^b \hat{c}_s + \hat{\rho}_g^b \hat{c}_g)(\hat{T}^{\circ} - \hat{T}^{\infty}). \tag{3B}$$

The heat released by combustion is equal to the heat of combustion multiplied by the change in solid partial density across the flame. This energy goes into flow work to expand the combustion products across the flame and increases the sensible heat of the phases. As in typical gas-phase combustion (deflagration), the heat release greatly exceeds the flow work, *ie*:

$$|\hat{e}_g^{\mathcal{F}} - \hat{e}_s^{\mathcal{F}}| \gg \frac{\hat{P}}{\hat{\rho}_g^u} \sim \hat{R}\hat{T}^{\infty}. \tag{4B}$$

Therefore, equation (3B) can be approximated as:

$$(\hat{\rho}_s^b \hat{c}_s + \hat{\rho}_g^b \hat{c}_g)(\hat{T}^{\circ} - \hat{T}^{\infty}) = (\hat{\rho}_s^u - \hat{\rho}_s^b)(\hat{e}_s^{\mathcal{F}} - \hat{e}_g^{\mathcal{F}}). \tag{5B}$$

In the case considered in the main text, we assume that a large fraction of combustion product is solid residual and therefore the thermal capacitance of the solid phase exceeds that of the gaseous combustion products, *i.e.* $\hat{\rho}_s^b \hat{c}_s > \hat{\rho}_g^b \hat{c}_g$. The thermal field of the reacted region is approximated by the spatially-uniform, adiabatic temperature:

$$\hat{T}^\circ = \hat{T}^\infty + \frac{(\hat{\rho}_s^u - \hat{\rho}_s^b)(\hat{e}_s^{\mathcal{F}} - \hat{e}_g^{\mathcal{F}})}{\hat{\rho}_s^b \hat{c}_s}. \tag{6B}$$

In the limit of total reactant consumption, only gas products reside in the reacted region and equation (6B) can not be used. For that case, the thermal field becomes nonuniform and the gasdynamics of the gases in the reacted region must be considered. Thus, the jump in energy across the flame must include the transport of energy into the reacted region.

11 Appendix C

Extension to High Reynolds Number Flow of Combustion Gases

The theory presented in the main text is restricted to low Reynolds number or Darcy flow of the product gas in the unreacted material. If the pore sizes in the granular reactant are large enough and the combustion pressures high enough, the Reynolds number based on interstitial velocity v and particle size d_p:

$$Re = \frac{\hat{\rho}_g \hat{v} \hat{d}_p}{\hat{\mu}_g}, \tag{C1}$$

will be large. Under these conditions, an additional term must be added to the drag law to account for inertial forces in the flow.

The modified drag law was first introduced by Ergun [15] and has the form

$$-\frac{\partial \hat{P}}{\partial \hat{x}} = \frac{\phi_g \hat{\mu}_g}{\hat{\kappa}} \hat{v} + \frac{\phi_g \alpha}{\hat{\kappa}} \hat{\rho}_g \hat{v}^2. \tag{C2}$$

The constant α is an empirically determined factor which is related to the pore size and shape and to the overall porosity. For packed beds of spheres with diameter d_p, α was found by Ergun to be:

$$\alpha = \frac{0.012 \hat{d}_p}{1 - \phi_g}. \tag{C3}$$

The purpose of this appendix is to reformulate the model equations given in the main text for the more general drag law described above. In particular, the limiting case of very high Reynolds number flow will be examined. We will derive the analytic solutions for the special cases of a steady boundary layer in moving coordinates and the quasi-steady flow between the flame and reactor exit. Numerical results for the general case are given for some representative Reynolds numbers.

Using the scaling scheme given in equation (14) of the main text, the non-dimensional equations governing gas flow in the region ahead of the flame are:

$$\frac{\partial P}{\partial t} + \frac{\partial (Pv)}{\partial x} = 0, \tag{C4}$$

and

$$-\kappa\frac{\partial P}{\partial x} = v + \mathcal{R}Pv^2, \tag{C5}$$

where $\mathcal{R}$ is a parameter which could be called a "characteristic Reynolds number" and is defined as

$$\mathcal{R} = \frac{\alpha(\hat{\rho}_s^u - \hat{\rho}_s^b)\hat{V}_F}{\hat{\mu}_g}. \tag{C6}$$

An alternative scaling which is more appropriate for high Reynolds number flow is based on a new constant σ defined as

$$\sigma = \frac{\kappa}{\mathcal{R}}. \tag{C7}$$

With only this substitution, the momentum equation is transformed to

$$-\sigma\frac{\partial P}{\partial x} = \frac{v}{\mathcal{R}} + Pv^2. \tag{C8}$$

The boundary condition at the flame is independent of the particular form of the scaling and is equivalent to equation (9) of the main text. In scaled variables, the form most convenient for this section is:

$$Pv|_{x=t} = 1 + \lambda P. \tag{C9}$$

A simplified form of the complete system of equations (C4), (C5) or (C8) , and (C9) can be found by using either (C5) or (C8) to eliminate the velocity from equations (C4) and (C9). For example, using the high Reynolds number scaling, equation (C5), the boundary condition can be rewritten as

$$-\sigma\frac{\partial P}{\partial x} = \frac{(1+\lambda P)}{\mathcal{R}} + (1+\lambda P)^2, \tag{C9a}$$

and the velocity can be determined by solving equation (C5) to obtain

$$Pv = \frac{1}{2}\left(\sqrt{\frac{1}{\mathcal{R}^2} + 4P\left(-\sigma\frac{\partial P}{\partial x}\right)} - \frac{1}{\mathcal{R}}\right). \tag{C5a}$$

Additional insight into the behavior of the solutions at high Reynolds number can be obtained by taking the limit $\mathcal{R} \to \infty$ in equations (C5a) and (C9a).

The resulting equations are:

$$Pv = \sqrt{P(-\sigma \frac{\partial P}{\partial x})}, \qquad (C5b)$$

and

$$-\sigma \frac{\partial P}{\partial x}|_{x=t} = (1 + \lambda P)^2, \qquad (C9b)$$

This system of equations is similar to the equivalent low Reynolds number model (equations (15) and (16) of the main text). Numerical solutions to this system of equations have been obtained for λ =0.5 and various σ . The computed pressure at the flame front is shown in Figure 14.

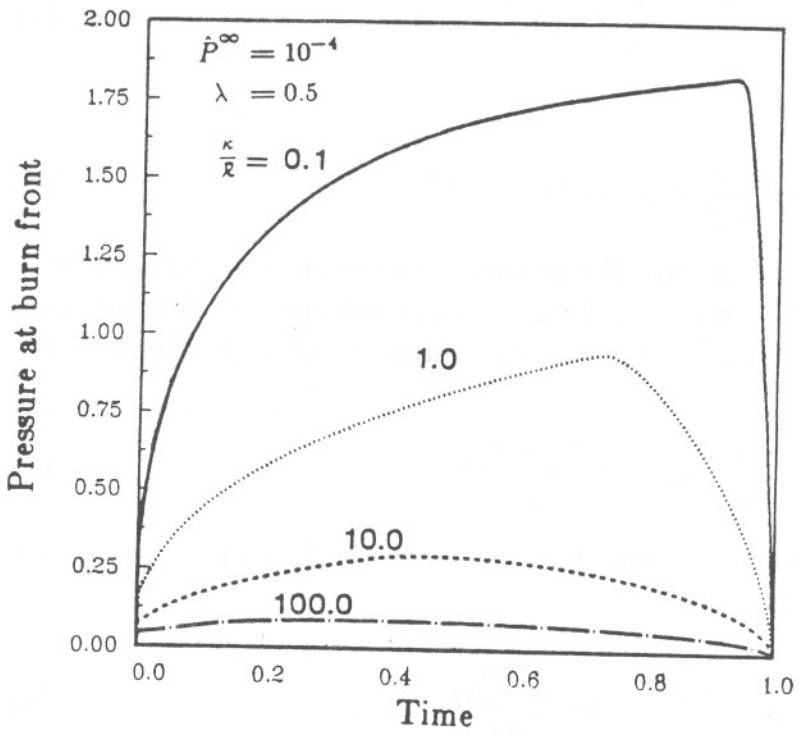

Figure 14. Numerical solutions of the pressure at the burn front for high Reynolds number gas flow.

The rest of this appendix will be devoted to examining approximate analytical solutions of (C5a) and (C9a). Closed-form solutions can be found for early times (a steady-state boundary layer in moving coordinates) and late times (quasi-steady flow between the flame front and the reactor exit).

First, the early-time solution will be presented. Since the bed is effectively semi-infinite at early times, σ can be eliminated by a transformation of variables. The equations can be solved in a coordinate system moving with the flame velocity and with the origin at the flame front. The necessary transformation is:

$$t' = \frac{t}{\sigma},$$

$$x' = \frac{(x-t)}{\sigma},$$

which yields the transformed equations

$$\frac{\partial P}{\partial t'} - \frac{\partial P}{\partial x'} + \frac{\partial}{\partial x'}(-P\frac{\partial P}{\partial x'})^{\frac{1}{2}} = 0, \qquad (C10)$$

and

$$-P\frac{\partial P}{\partial x'}|_{x'=0} = (1+\lambda P)^2. \qquad (C11)$$

To simplify the notation, we will drop the primes on the transformed variables. First, we determine the traveling wave solutions which are independent of time, *ie*, $\frac{\partial}{\partial t} = 0$. The structure of the steady-state permeation layer in front of the flame is determined by:

$$\frac{\partial P}{\partial x} = \frac{\partial}{\partial x}(-P\frac{\partial P}{\partial x})^{\frac{1}{2}}. \qquad (C14)$$

A single integration of this equation, with the boundary condition (C11) at $x = 0$ and $\frac{\partial P}{\partial x} \to 0$ as $x \to \infty$, yields:

$$P - P^{\infty} = (-P\frac{\partial P}{\partial x})^{\frac{1}{2}}, \qquad (C14a)$$

and as in the low Reynolds number case (*cf.*, equation (30)), the maximum pressure at the flame front is

$$P^{\circ}_{max} = \frac{1+P^{\infty}}{1-\lambda}.$$

Using the scaling defined in Section 6 of the main text (*cf.*, equations (32) , (34))

$$\psi = \frac{P - P^{\infty}}{P^{\circ}_{max} - P^{\infty}}$$

equation (C14a) can be recast to the following form:

$$\psi^2 + (\psi + \epsilon)\frac{\partial \psi}{\partial x} = 0, \qquad (C15)$$

where ϵ is the same parameter defined in the main text (equation (33)):

$$\epsilon = \frac{P^{\infty}}{P^{\circ}_{max} - P^{\infty}}.$$

Equation (C15) can be integrated to give a closed-form solution analogous to equation (35) of the main text:

$$\ln \psi - \epsilon(1 + \frac{1}{\psi}) = -x. \qquad (C16)$$

In the limit $\epsilon \rightarrow 0$ (*ie*, very high pressure at the flame front compared to the ambient pressure), the solution is:

$$\psi = \exp(-x). \qquad (C17)$$

In terms of the physical, dimensional variables, the boundary layer has a thickness (based on $\psi = \exp(-1)$) of $\delta = \sigma$. The characteristic time required for the boundary layer to develop will be $\tau = O(\frac{\sigma}{V_F})$. There is an additional, unspecified dependence on λ that can be determined by numerical solution of the time-dependent equations in a moving coordinate system. This could be carried out by an approximate integral approach similar to that described in Section 6. The functional dependence of pressure on distance should probably be chosen as exponential, as suggested by equation (C17), rather than the linear dependence chosen for the low Reynolds number case.

The second type of closed-form solution which can be obtained is valid at late times, after the permeation layer has contacted the end of the reactor and a quasi-steady gas flow has developed between the flame front and the bed exit. The analysis for this situation is identical to that carried out in the main text. In fact, the only difference in the result is that the pressure at the bed exit is

given by a different expression. The governing equations are equation (41) of the main text:

$$(P^2 - P^{\infty 2}) = (P^{\circ 2} - P^{\infty 2})(1 - \frac{(x-t)}{(1-t)}),$$

equation (43) of the main text

$$\dot{m} = (1 + \lambda P^{\circ}),$$

and the pressure at the flame front is given by the positive root of the following quadratic:

$$(1 + 2\frac{\lambda^2}{\sigma}(1-t))P^{\circ 2} + (4\frac{\lambda}{\sigma}(1-t))P^{\circ} - (P^{\infty 2} - \frac{2}{\sigma}(1-t)) = 0. \qquad (C18)$$

12 Appendix D

Complete Gasification of Reactants

Near the limit of complete gasification of the solid phase reactants, the temperature field becomes nonuniform and a spatial variation of gas density induces a flow of product gas within the reacted region. To treat this flow field we use a model of the gasdynamics derived in the limit of slow combustion. The gasdynamic equations relevant to this limit were first derived by Sivashinsky [1] and the interested reader should consult this reference for details of the theory.

In considering an isentropic flow of ideal product gas which has an adiabatic index, γ, the conservation of gas mass within the confined reacted region is given by:

$$\frac{\partial v_g}{\partial x} = -\frac{1}{\gamma P^\circ}\frac{dP^\circ}{dt}, \tag{D1}$$

where the pressure field within the reacted region changes only temporally.

For one-dimensional planar flow into a linearly expanding reacted region, the flow velocity of hot gases (normalized by the burn velocity of the porous reactant) at the flame front is given as:

$$v_g^b = -\frac{t}{\gamma P^\circ}\frac{dP^\circ}{dt}. \tag{D2}$$

With the forementioned relationship, the balance of mass across the flame is modified and the nondimensionalized relationship is given as:

$$-\kappa P^\circ \frac{\partial P^\circ}{\partial x} + \frac{t(1-\lambda)}{\gamma}\frac{dP^\circ}{dt} = 1 + \lambda P^\circ. \tag{D3}$$

As defined in the main text, $1-\lambda$ is related inversely to the gas temperature ratio across the flame and the jump in energy determines its value. Rather than being a fixed value (as was considered in the main text), λ will vary with the pressure at the burn front. Isentropic compression of the combustion product gases is represented by the following relationship:

$$(1-\lambda) = (1-\lambda_o)\left(\frac{P^\infty}{P^\circ}\right)^{(1-\frac{1}{\gamma})}, \tag{D4}$$

where λ_o refers to the initial combustion condition $P^\circ = P^\infty$.

To demonstrate the importance of including the gasdynamics of the product region flow we present two sets of numerical calculations of the pressure at the burn front shown in Figure 15 using model constants $\lambda_o = 0.5$ and $\gamma = 1.2$. The solid curves correspond to an isothermal product region calculation using the model described in the main text and the broken curves are comparable cases for isentropic flow of the product gases using the boundary constraint of equation (D3). Two permeabilities , $\kappa = 0.1$ and 10., are examined.

For low permeability, numerical calculations indicate that the flow in the product region is important. Higher pressures are seen to develop when compression of the gas phase is included in the model. For highly permeable materials, the isentropic and isothermal models yield similar predictions of the pressure at the burn front.

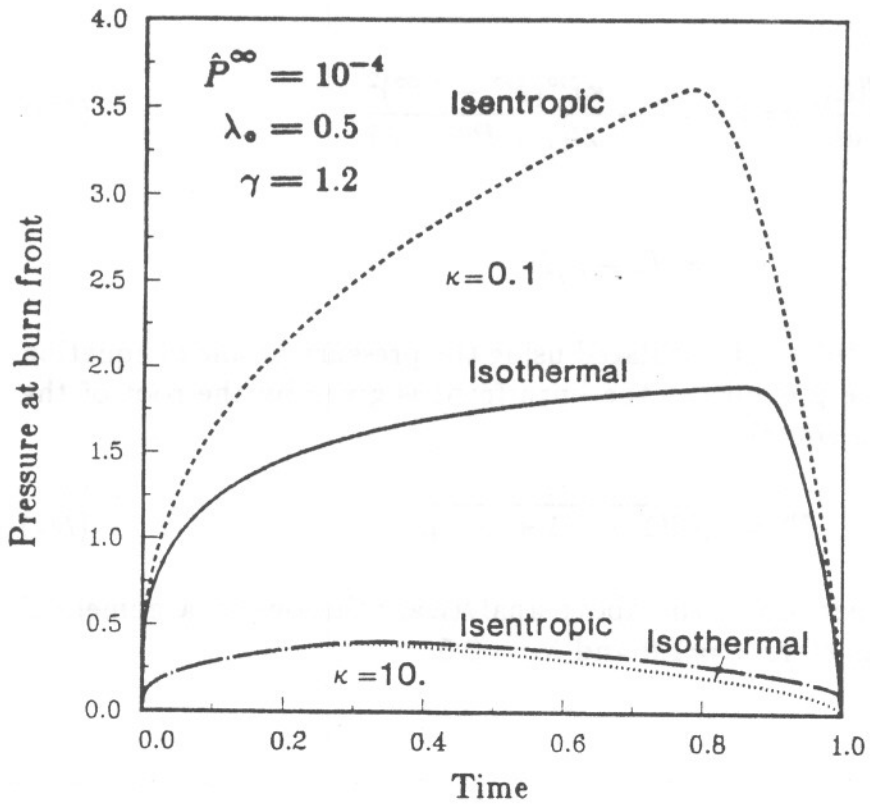

Figure 15. Comparison of the temporal variation of burn front pressure with isentropic gas flow in the confined reacted region to that without gas flow in the confined reacted region.

Approximate analytical solutions have also been determined for this case using the same methods outlined in the main text. The early-time behavior can be approximated using the boundary layer integral method. Using the pressure wave forms given by equation (39) in the main text, the pressure at the burn front, P° , and the boundary layer thickness, δ , are determined by:

$$\frac{(P^\circ - P^\infty)\delta}{2} = t(1 + P^\infty - \Lambda), \tag{D5}$$

and

$$\frac{d(t\Lambda)}{dt} = 1 + P^\circ - \frac{\kappa P^\circ (P^\circ - P^\infty)^2}{2t(1 + P^\infty - \Lambda)}, \tag{D6}$$

where

$$\Lambda = (1 - \lambda)P^\circ.$$

The quasi-steady solution is calculated using the pressure profile of equation 41 of the main text. The pressure at the burn front is given by the root of the following transcendental equation:

$$P^\circ = \sqrt{2(1-t)(1+\lambda P^\circ)}. \tag{D7}$$

Figure 16 shows a comparison of the above analytical solutions to a numerical solution for model parameters κ =1.0 and λ_o =0.5.

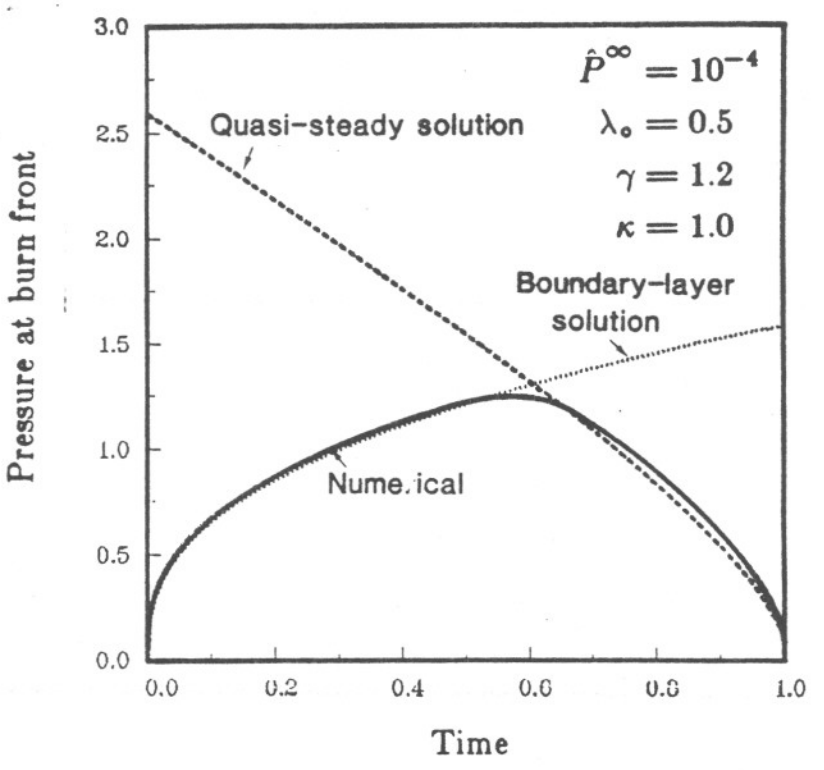

Figure 16. Comparison of analytical solutions to numerical calculations of the pressure at the burn front for complete gasification of the reactant.

DISTRIBUTION:

Prof. H. Krier
Department of Mechanical Engineering
University of Illinois
Champaign, Il 61820

Sandia Internal:

1510 J. W. Nunziato
1511 G. G. Weigand
1511 G. R. Hadley
1511 K. L. Erickson
1512 J. C. Cummings
1512 D. A. Benson
1512 A. W. Reed
1512 J. E. Shepherd (10)
1513 D. W. Larson
1513 M. R. Baer (10)
1513 S. K. Griffiths
1513 R. J. Gross
1520 D. J. McCloskey
1530 L. W. Davison
1540 W. C. Luth
2510 D. H. Anderson
2513 J. E. Kennedy
2530 D. B. Hayes
8120 L. D. Bertholf
8125 M. John
8125 G. Evans
8125 W. Hermina
8231 R. Kee
8231 S. B. Margolis
8314 W. Hoover
8343 C. F. Melius
8424 M. A. Pound
8521 D. Hardesty
3141 C. M. Ostrander (5)
3151 W. L. Garner (3)
for DOE/TIC
3154-4 C. Dalin (25)